Effect of heat treatment on microstructure and thermal properties of Cu-based shape memory ribbons

Kožuh, Stjepan; Ivanić, Ivana; Holjevac Grgurić, Tamara; Gojić, Mirko

Source / Izvornik: **Kemija u industriji : Časopis kemičara i kemijskih inženjera Hrvatske, 2022, 71, 591 - 600**

Journal article, Published version
Rad u časopisu, Objavljena verzija rada (izdavačev PDF)

https://doi.org/10.15255/KUI.2022.011

Permanent link / Trajna poveznica: https://urn.nsk.hr/urn:nbn:hr:115:190654

https://doi.org/10.15255/KUI.2022.011
KUI-49/2022
Original scientific paper
Received February 16, 2022
Accepted April 27, 2022

Effect of Heat Treatment on Microstructure and Thermal Properties of Cu-based Shape Memory Ribbons

S. Kožuh,[a*] *I. Ivanić*,[a] *T. Holjevac Grgurić*,[b] and *M. Gojić*[a]

[a] University of Zagreb, Faculty of Metallurgy, Aleja narodnih heroja 3, 44 000 Sisak, Croatia
[b] Catholic University of Croatia, Ilica 242, 10 000 Zagreb, Croatia

Abstract

The aim in this work was to investigate the change in microstructure, phase transformation temperatures, and thermal properties due to the quenching of the investigated Cu-Al-Mn and Cu-Al-Mn-Ti alloys in ribbon form. This paper presents the results of microstructure analysis and thermal properties of Cu-Al-Mn and Cu-Al-Mn-Ti shape memory alloys produced in ribbon form by melt spinning technique. The microstructural analysis was carried out before and after quenching. After casting of the investigated alloys, annealing at 900 °C for 30 min was performed, followed by water quenching. The microstructural analysis was carried out by optical and scanning electron microscopy equipped with an energy dispersive spectrometer and by X-ray diffractometer. Thermodynamic calculation of a ternary Cu-Al-Mn system in equilibrium condition was performed using Thermo-Calc 5 software. Phase transformation temperatures were determined by differential scanning calorimetry and electrical resistance measuring. The results of microstructural analysis show the presence of martensite microstructures before and after quenching in the Cu-Al-Mn alloy, while in the Cu-Al-Mn-Ti alloy martensite microstructure exists only after quenching. Phase transformation temperatures decreased after quenching and titanium addition.

Keywords

Cu-Al-Mn, Cu-Al-Mn-Ti, shape memory alloys, microstructure characterisation, thermal analysis, X-ray spectroscopy

1 Introduction

Commercially attractive shape memory alloys (SMAs), such as copper-based shape memory alloys, have practical applications because of their characteristic properties, *i.e.*, superelasticity (SE), shape memory effect (SME), two-way memory effect (TWME), and damping properties.[1] In addition, alloys like Ni-Ti with shape memory effect can be used in different ways to control civil structures.[2] Usually these alloys can be used in the form of bars, wires or plates. *Mali et al.*,[2] in their review on shape memory alloys, concluded that SMAs have many opportunities and represent the construction materials of the future. *Quader et al.*[3] stated that there are different techniques available to shape memory alloys production: (i) casting – vacuum arc remelting, vacuum induction melting or electron beam melting, (ii) powder metallurgy – conventional processes or additive manufacturing.

Compared to other shape memory alloys, copper-based alloys have the following main advantages: (i) lower cost than nickel-based alloys, and (ii) better SME and SE properties than iron-based alloys. Copper-based shape memory alloys are easier to produce than nickel-based alloys, and are less expensive. However, a great disadvantage of some copper-based shape memory alloys, like Cu-Al-Ni or Cu-Zn-Al, is brittleness and insufficient cold-working. Improvement of ductility has been achieved with the addition of manganese, so Cu-Al-Mn with low aluminium content shows good ductility. Practical applications of Cu-Al-Mn shape memory alloys can be applied as SE, SME, and TWME materials, as high damping material or as material with high thermal and electrical conductivities, *e.g.*, for medical and electrical devices.[1] The reason for this application is microstructure and texture control such as grain size. *Hasnat el al.*[4] gave a review of utilising shape memory alloy in structural safety. In their work, they concluded that the production of SMAs and devices based on SMAs was still comparatively expensive, which could be main reason for restriction of application of this alloy in structural engineering. Civil engineering structures are often very large and require a lot of material. According to literature,[5] Cu-Al-Mn SMAs are appropriate for application in civil engineering because of their high damping capacity. *Kumar et al.*[6] in investigations of changes in properties of Cu-Al-Mn shape memory alloys mentioned that quaternary addition of different elements can have a significant effect on alloy properties. Adding some alloying elements, such as Mn, Ti, Fe, Zr, and B can significantly improve mechanical properties, especially ductility.[7–8] In addition, the addition of manganese has been proven to enhance thermoelastic and pseudoelastic behaviours. Magnetic properties can be a function of the addition of a fourth element (*e.g.*, Ag, Be, Co, Ga, Sb or Zr).[9]

The behaviour of shape memory alloys is significant under various thermal conditions due to the development of martensite that occurs in these alloys. The Ni-Ti alloys were often exposed to heat treatment (annealing) at 550 °C in order to create conditions with a recovered microstructure in comparison to cold-working conditions.[10] On the other hand, the Cu-based shape memory alloys are usually annealed in β-region at 800 or 900 °C to achieve preconditions for the formation of shape memory effect.[10,11] *Canbay et al.*[12] mentioned that copper-based shape memory alloys

* Corresponding author: Prof. Stjepan Kožuh, PhD
Email: kozuh@simet.unizg.hr

show transformation to martensite on cooling, and transformation to austenite on heating, and during the cooling process close packed structures are characterised by order, such as 6R, 18R, and 2H type. It is known that, in Cu-Al-Mn shape memory alloys, there exists the disordered β-phase which is stable at high temperatures. This phase transforms into martensite with quenching. Transformation is started by reactions: $\beta(A2) \rightarrow \beta_2(B2) \rightarrow \beta_1(L2_1)$.[13] At the end of transformation, three different types of martensite can be formed: $\alpha_1'(3R)$, $\beta_1'(18R)$ and $\gamma_1'(2H)$. Ordered structures, like $B2^-$, DO_3^- or $L2_1$, transform into close-packet martensite structures (6R, 18R and 2H) with cooling. The type of martensite depends on alloy composition. Type β_1' martensite is predominant at lower aluminium content, while type γ_1' is mainly formed at higher content of aluminium. In addition, β_1' and γ_1' martensites co-exist in the intermediate range. *Canbay et al.*[14] characterised ternary 82.20 Cu – 12.67 Al – 3.13 Mn (wt.%), and obtained presence of both types of 18R and 2H martensite phases. In addition, *Canbay et al.*[15] mentioned that aging process has significant effect on transformation temperatures. The alloys show SME because the martensite re-orientation under external force causes a thermoelastic martensite transformation. *Mallik et al.*[16] mentioned that Zn and Ni, as quaternary additions, increase the martensite transformation temperatures, while Fe, Cr, Si, Mg, and Ti decrease them.

2 Experimental

2.1 Materials

The Cu-Al-Mn and Cu-Al-Mn-Ti shape memory ribbons used in this investigation were cast by the melt spinning process. Production of the investigated alloys was performed using technically pure components: Cu (purity 99.9 %), Al (purity 99.5 %), Mn (purity 99.8 %), and Ti (purity 99.8 %). Certain weights of the pure components were re-melted by induction melting in a graphite crucible. The produced Cu-Al-Mn and Cu-Al-Mn-Ti ingots were used as input material for ribbon productions. The dimensions of solidified ingots were ϕ45×55 mm and about 680 g in weight. The ingots were smelted and injected through a rectangular nozzle onto a cold surface of the melt spinner. The melting temperature of the ingots was around 1450 °C. Under argon overpressure in the graphite crucible, the molten alloy was sprayed through the nozzle on a rotating disc made of copper alloy. Because of very fast heat transfer, ribbons with width 3.5–5.0 mm and thickness 0.12–0.30 mm were produced. The chemical composition of the produced alloys is presented in Table 1.

Table 1 – Chemical composition of investigated Cu-Al-Mn and Cu-Al-Mn-Ti shape memory alloys

Tablica 1 – Kemijski sastav istraživanih Cu-Al-Mn i Cu-Al-Mn-Ti legura s prisjetljivosti oblika

Alloy Legura	Chemical composition / wt.% Kemijski sastav / mas. %			
	Cu	Al	Cu	Ti
Cu-Al-Mn	83.77	8.79	7.44	–
Cu-Al-Mn-Ti	87.04	5.74	6.77	0.45

2.2 Methods

After casting, the ribbons were solution annealed at 900 °C in the electro-resistance chamber furnace for 30 min, and then quenched in room-temperature water. The investigated alloys were heated at 900 °C in order to carry out the quenching in water from high-temperature β phase region, and thus create the preconditions for the formation of martensite. Microstructural characterisation of samples was carried out by optical microscopy (OM) using an Olympus GX 71s, scanning electron microscopy (SEM) using TESCAN VEGA 5136MM equipped with a device for energy dispersive spectroscopy (EDS) (measurement conditions: SEI, HV = 20.00 kV, WD = 20.00 mm), and X-ray diffraction (XRD) analysis by Shimadzu XRD 6000 diffractometer (measurement conditions: 40.0 kV, 30.0 mA, scan range 2θ: 20–100°). The samples for metallographic analysis were prepared by mechanical grinding (papers 120–1200) and polishing (water suspension of 0.3 μm Al_2O_3), and were then etched using a solution of 2.5 g $FeCl_3$, 48 ml methanol, and 10 ml HCl. XRD analysis was done with CuKα radiation on a Philips PW 1830 to identify the phases present in the samples.

Thermodynamic calculation for Cu-Al-Mn was carried out by Thermo-Calc software based on the CALPHAD method. Thermal properties were analysed on a Mettler Tolledo 822e differential scanning calorimeter (Mettler Toledo, Greifensee, Switzerland). The samples were tested in a temperature range from –100 to 250 °C in two heating/cooling cycles at a rate of 10 °C min^{-1}, under N_2 atmosphere, (40 ml min^{-1}). The heating/cooling rate of 10 °C min^{-1} was applied for DSC measurements because it is a standard heating/cooling rate for metal samples analysis and determination of transformation temperatures. For the measurement of electrical resistance, the D.C. method was used. By this method, the ribbons were coiled on a 50 mm long ceramic tube. During the heating period, the electrical resistance was measured in the tube furnace, and temperature change was observed by the thermocouple Pt-Pt 10% Rh. The heating from room temperature up to 200 °C was controlled by the Eurotherm control system. The electrical resistance was simultaneously calculated at known electric current through the sample and a measured voltage drop.

3 Results and discussion

3.1 Microstructural characterisation

Optical micrographs of Cu-Al-Mn alloy before and after quenching show a certain increase in grain size in quenching state (Figs. 1 and 2). Optical micrographs of the Cu-Al-Mn-Ti alloy before quenching show a significantly different microstructure than the Cu-Al-Mn alloy. The Cu-Al-Mn alloy before and after quenching shows the presence of a martensitic microstructure. In contrast, Cu-Al-Mn-Ti alloy optical micrographs cannot detect the formation of

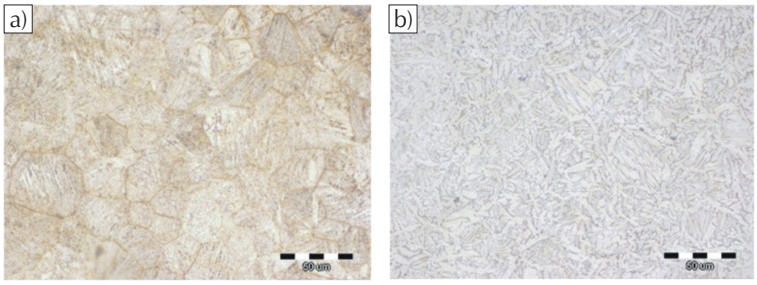

Fig. 1 – Optical micrographs of Cu-Al-Mn (a) and Cu-Al-Mn-Ti (b) shape memory ribbons before quenching

Slika 1 – Optičke mikrografije Cu-Al-Mn (a) i Cu-Al-Mn-Ti (b) traka s prisjetljivosti oblika prije kaljenja

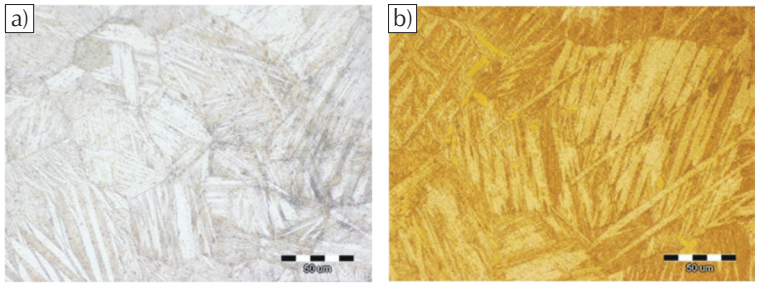

Fig. 2 – Optical micrographs of Cu-Al-Mn (a) and Cu-Al-Mn-Ti (b) shape memory ribbons after quenching

Slika 2 – Optičke mikrografije Cu-Al-Mn (a) i Cu-Al-Mn-Ti (b) traka s prisjetljivosti oblika nakon kaljenja

martensite before quenching (Fig. 1). By annealing and quenching (900 °C/30 min/water), a martensitic microstructure was achieved (Fig. 2).

More detailed microstructural characterisation was performed by scanning electron microscopy and energy dispersive spectroscopy. The SEM micrographs of the Cu-Al-Mn and Cu-Al-Mn-Ti alloys before and after quenching are shown in Figs. 3 and 4, and the obtained images confirm the results of optical microscopy. The Cu-Al-Mn alloy before quenching shows the presence of the martensitic microstructure and the partial regions of the untransformed β phase. A similar microstructure was observed in the quenched state of the Cu-Al-Mn alloy. The SEM micrographs show the presence of a lath type (β_1') martensite with thin plates in quenched Cu-Al-Mn alloy. The Cu-Al-Mn-Ti alloy before quenching shows no presence of martensite, and its microstructure consists of a two-phase region of $\alpha + \beta_1$. Grain structure with $\alpha + \beta$ phase, before quenching, clearly indicates that this alloy has potential to exhibit the martensite formation and shape memory behaviour after quenching. By annealing at 900 °C, a single-phase β_1 structure of Cu-Al-Mn-Ti alloy was produced, and by quenching, it transformed into martensite. Quenching at 900 °C was carried out expecting formation of martensitic microstructures. This formation was observed in both quenched samples. Moreover, in the microstructure, the presence of residual untransformed β_1 phase can be observed. If copper-based shape memory alloys are exposed to cooling below the critical martensite start temperature, martensite can be formed as plates.[17] The structure of martensite is caused by martensite variants. In the beginning, the individual plates of martensite are very thin or parallel. Usually, martensite grows in broader units, which consist of two or four plates. It is known from literature[18] that Cu-Al-Mn alloys can undergo martensitic transformation from the β phase, which is stable at high temperatures. During quenching from β region transformation β (A2) $\rightarrow \beta_2$ (B2) $\rightarrow \beta_1$ ($L2_1$) occurs. In this case, three forms of martensite can arise from the β_1 phase: α'(3R), β_1'(18R) and γ_1'(2H), which depends on the aluminium and manganese content. At lower aluminium content, β_1' martensite is usually dominant. In contrast, higher aluminium content produces γ_1' martensite. For the range between higher and lower content of aluminium and manganese, there are β_1' and γ_1' martensite at the same time. *Mielzarek et al*.[19] concluded that, below approximately 500 °C, Cu-Al-Mn has an ordered structure of $L2_1$ (bcc) that transforms into 18R, which can be observed as small acicular martensite or 2H, which can be observed as large acicular martensite. *Hussain et al*.[20] also investigated the Cu-Al-Mn-Ti alloy, and found the existence of a two-phase $\alpha + \beta$ region in casted state. By quenching these alloys, they observed a similar effect, *i.e.*, the formation of martensite β_1', and γ_1', respectively. *Gerdan et al*.,[21] in their investigation of martensite transformation, concluded that the microstructures of Cu-Al-Mn and Cu-Al-Mn-Zn alloys consisted of β_1' martensite (thinner phase), and γ_1' martensite (thicker phase), and in both alloys they observed no formation of precipitates. It is known that the addition of titanium to Cu-Al-Mn alloys results in grain refining.[20] By addition of titanium and with the formation of martensite after quenching, a slightly finer grain in Cu-Al-Mn-Ti alloys can also be observed.

The martensite microstructure can have two different morphologies: needle-like and plate-like.[22] β_1' and γ_1' phases are two types of thermal-induced martensites, and γ_1' phase forms as coarse variants, *i.e.*, plate-like phase. In contrast, β_1' is a phase that forms as a needle-like phase and usually arises between γ_1' phase. Figs. 2 and 4 show that self-accommodated plate-like martensites nucleate and grow mostly in a different direction.

The EDS analysis of the chemical composition of Cu-Al-Mn and Cu-Al-Mn-Ti alloys at different positions is presented in Tables 2 and 3. By detailed analysis of the EDS results of the Cu-Al-Mn alloy, it can be concluded that a homogeneous alloy was produced by melt spinning technique. In the casted state, the copper content was 83.22–84.23 %, aluminium 8.44–9.37 %, and manganese 7.33–7.59 %. After quenching of Cu-Al-Mn alloy, insignificant changes in the chemical composition of the investigated positions were observed. These minor changes in chemical composition can be explained by EDS device error. The EDS analysis of the Cu-Al-Mn-Ti alloy also shows the achievement of a homogeneous composition in casted state (Cu: 86.51–87.24 %; Al: 5.56–5.91 %; Mn: 6.53–7.28 % and Ti:

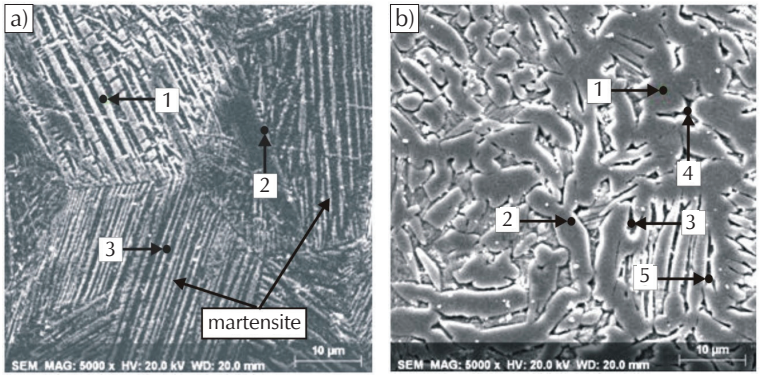

Fig. 3 – SEM micrographs of Cu-Al-Mn (a) and Cu-Al-Mn-Ti (b) shape memory ribbons before quenching with marked positions for EDS analysis

Slika 3 – SEM mikrografije Cu-Al-Mn (a) i Cu-Al-Mn-Ti (b) traka s prisjetljivosti oblika prije kaljenja s označenim pozicijama za EDS analizu

0.40–0.55 %, in wt.%; Table 2). In addition, similar values of EDS analysis were obtained for the quenched state of Cu-Al-Mn-Ti alloy (Table 3).

Figs. 5 and 6 show the XRD results of the investigated alloys before and after quenching. The major probable peaks were determined and marked in Figs. 5 and 6. The martensitic microstructures $AlCu_3$ (β_1') and Al_4Cu_9 (γ_1') were clearly determined. The XRD results of the Cu-Al-Mn alloy before quenching showed that the microstructure consisted of austenite (β_1 phase) and two martensite (β_1' and γ_1') microstructures. In contrast, the Cu-Al-Mn-Ti alloy before quenching showed the presence of two phases in the microstructure, but without martensite. Thus, the microstructure of the Cu-Al-Mn-Ti alloy before quenching consisted of austenite (β_1 phase) and α phase (Cu FCC). It is known that,

Table 2 – EDS results of Cu-Al-Mn (a), and Cu-Al-Mn-Ti (b) shape memory ribbons before quenching; positions marked in Fig. 3

Tablica 2 – EDS rezultati Cu-Al-Mn (a) i Cu-Al-Mn-Ti (b) traka s prisjetljivosti oblika prije kaljenja; pozicije označene na slici 3

Alloy Legura	Position Pozicija	Chemical compositions / wt.% Kemijski sastav / mas. %			
		Cu	Al	Mn	Ti
Cu-Al-Mn (Fig. 3a) (slika 3a)	1	83.22	9.37	7.41	–
	2	84.23	8.44	7.33	–
	3	83.85	8.56	7.59	–
Cu-Al-Mn-Ti (Fig. 3b) (slika 3b)	1	87.20	5.72	6.53	0.55
	2	87.18	5.56	6.85	0.41
	3	87.08	5.91	6.60	0.40
	4	86.51	5.77	7.28	0.44
	5	87.24	5.76	6.57	0.43

Table 3 – EDS results of Cu-Al-Mn (a), and Cu-Al-Mn-Ti (b) shape memory ribbons after quenching; positions marked in Fig. 4

Tablica 3 – EDS rezultati Cu-Al-Mn (a) i Cu-Al-Mn-Ti (b) traka s prisjetljivosti oblika nakon kaljenja; pozicije označene na slici 4

Alloy Legura	Position Pozicija	Chemical compositions / wt.% Kemijski sastav / mas. %			
		Cu	Al	Mn	Ti
Cu-Al-Mn (Fig. 4a) (slika 4a)	1	83.29	9.48	7.23	–
	2	84.67	8.74	7.60	–
	3	84.00	8.64	7.36	–
Cu-Al-Mn-Ti (Fig. 4b) (slika 4b)	1	87.64	5.38	6.63	0.36
	2	86.21	6.21	7.12	0.46
	3	85.49	7.07	7.02	0.41
	4	85.98	6.57	7.11	0.34

at temperatures below 500 °C, Cu-Al-Mn has a two-phase microstructure (α phase with FCC, and β phase with $L2_1$).[23] At a temperature higher than 550 °C, only a single β phase is present in the structure. The absence of martensite in Cu-Al-Mn-Ti alloy before quenching was confirmed by both optical and scanning electron microscopy (Figs. 1 and 3). The XRD results showed that there was no change in the microstructure of the Cu-Al-Mn alloy before and after quenching. The XRD analysis of Cu-Al-Mn alloy after quenching also showed the presence of β_1 phase (austenite) and β_1' phase (martensite), as in the case of the casted state. However, a more significant change could be observed on the X-ray patterns of the Cu-Al-Mn-Ti after quenching. The XRD analysis of quenched Cu-Al-Mn-Ti alloy showed the presence of three phases: β_1 phase (austenite), β_1'

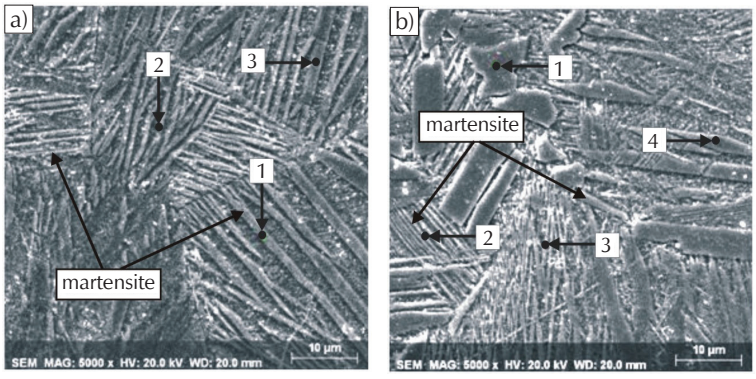

Fig. 4 – SEM micrographs of Cu-Al-Mn (a), and Cu-Al-Mn-Ti (b) shape memory ribbons after quenching with marked positions for EDS analysis

Slika 4 – SEM mikrografije Cu-Al-Mn (a) i Cu-Al-Mn-Ti (b) traka s prisjetljivosti oblika nakon kaljenja s označenim pozicijama za EDS analizu

phase (martensite), and γ_1' (martensite). The presence of β_1' and γ_1' martensites was also determined in Cu-Al-Mn-Ti ingots after quenching by investigation of *Mallik et al*.[16] The presence of martensite β_1'(18R) and γ_1'(2H) coincides with the results of DSC analysis, where in Cu-Al-Mn-Ti alloy after quenching, the presence of two exothermic peaks was observed on the cooling curve. These peaks can be associated with the formation of β_1' and γ_1' martensites.

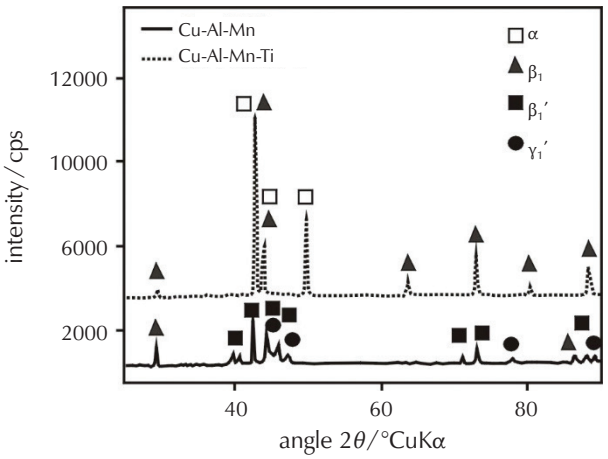

Fig. 5 – XRD patterns of Cu-Al-Mn and Cu-Al-Mn-Ti shape memory alloys before quenching
Slika 5 – XRD difraktogrami Cu-Al-Mn i Cu-Al-Mn-Ti legura s prisjetljivosti oblika prije kaljenja

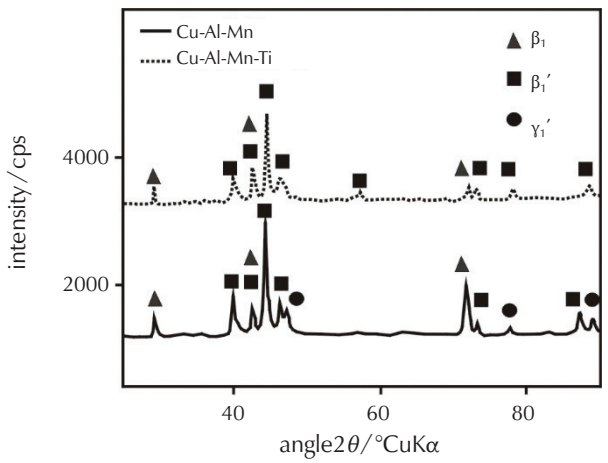

Fig. 6 – XRD patterns of Cu-Al-Mn and Cu-Al-Mn-Ti shape memory alloys after quenching
Slika 6 – XRD difraktogrami Cu-Al-Mn i Cu-Al-Mn-Ti legura s prisjetljivosti oblika nakon kaljenja

3.2. Thermal properties

Thermodynamic calculation for Cu-Al-Mn was carried out by Thermo-Calc software based on the CALPHAD method and minimisation of Gibbs energy. Fig. 7 shows the vertical section of calculated phase diagram with Cu 85 wt.%-Mn 7 wt.%-Al. Calculation of phase diagram was performed according to optimised parameters for ternary system Cu-Al-Mn by *Miettinen*[24] in Cu-rich region. The disorder-order phase transitions of β-phase A2 → B2 → L21 were not taken in the Miettinen calculations due to lack of data. It is well known that, under fast cooling, metastable martensitic phases β'(18R), γ_1'(2H) or α'(3R) can be formed depending on the component composition. In Fig 7, a narrow area of stability of pure β-phase (BCC_A2) can be seen, and precipitation of α-phase (FCC_A1) at 890 °C. Below 470 °C, the ternary phase starts to precipitate, tau 3 phase, Cu_3Mn_2Al, and at room temperature, stability of two-phase region Cu_3Mn_2Al + α-phase (FCC_A1) can be noticed. At higher contents of aluminium in Cu-Al-Mn, a stable region Cu_3Mn_2Al + α-phase + γ-phase at low temperatures can be observed, as well as eutectoid reaction at 393 °C.

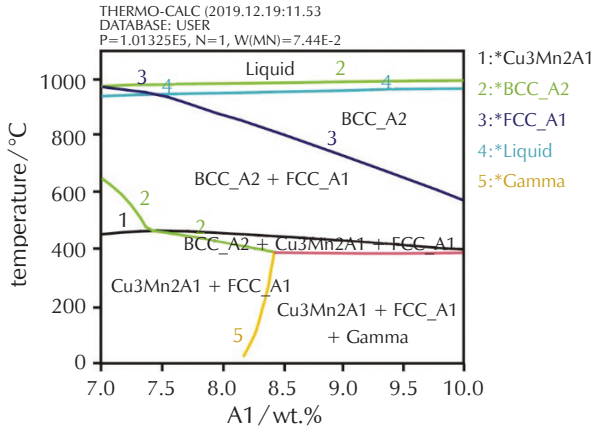

Fig. 7 – Vertical section of calculated phase diagram for Cu 85 wt.%-Mn 7 wt.%-Al
Slika 7 – Vertikalni presjek proračunatog faznog dijagrama za Cu 85 mas. %-Mn 7 mas. %-Al

Phase transformation behaviour was analysed with DSC measurements for heating and cooling. The heating/cooling rate was 10 °C min^{-1}, and the obtained DSC curves of the investigated alloys are shown in Figs. 8 and 9. Differential scanning calorimetry of the Cu-Al-Mn and Cu-Al-Mn-Ti alloys before and after quenching determined the temperature values of the start (onset) and finish (endset) of austenite formation, as well as martensite formation. The peaks are more pronounced in some transformations and less pronounced in others. A more detailed analysis of the DSC thermogram of the Cu-Al-Mn alloy before quenching showed two exothermic peaks on the cooling curve (Fig. 8a). Both of these points represent a martensite transformation, but it can be concluded that two different types of martensite occurred. The characteristic temperatures of transformation (A_s, A_f, M_s, and M_f) were determined from Figs. 8 and 9, and are given in Table 4. Before quenching of Cu-Al-Mn alloy, the start temperature of austenite formation (A_s) is at 89.06 °C and finish temperature (A_f) at 103.43 °C. The martensite formation started at temperature 82.97 °C (M_s), and the martensite finish temperature was 12.39 °C (M_f). After quenching of Cu-Al-Mn alloys, austenitic transformation started and finished at significantly lower temperature (Table 4). In the case of the quenched Cu-Al-Mn alloy, only one exothermic peak

can be observed on the cooling curve, which represents a martensitic transformation (Fig. 9a). The austenite formation start temperature for the Cu-Al-Mn-Ti alloy before quenching was 11.31 °C, and the transformation finished at 39.13 °C. The start temperature of the martensite formation was 37.23 °C, and finished at –12.10 °C, which is a similar behaviour with the casted Cu-Al-Mn alloy. The Cu-Al-Mn-Ti alloy before quenching also exhibited two exothermic peaks on the cooling curve (Fig. 8b, Table 4). It is probably also the case of the formation of two different forms (structures) of martensite. DSC analysis showed that, despite low intensity, martensite still formed in the as-cast state, with M_s at 37.23 °C and M_f at –12.10 °C. Since the formation of martensite structure had only just begun, that is probably the reason why martensite was not observed in SEM and OM micrographs. The quenched Cu-Al-Mn-Ti alloy achieved the start temperature of austenitic transformation at 8.33 °C and finished at 34.08 °C. The start temperature of the martensite formation was at 37.57 °C, and the martensite finished at –9.57 °C (complete martensite microstructure). In contrast to the quenched Cu-Al-Mn alloy, in the case of the quenched Cu-Al-Mn-Ti alloy, two types of martensite are visible on the cooling curve (Fig. 9b). These results indicate that the values of transformation temperatures for austenite and martensite microstructures vary with addition of titanium. In other investigations[25–28] of ductile Cu-Al-Mn shape memory alloys, the authors mentioned that transformation temperatures can be in a range from –200 to 150 °C; *e.g.*, *Zhou et al*.[26] in their investigation of Cu-8.7Al–10.8Mn alloy determined that M_s, M_f, A_s, and A_f at the top of the sample were 7.0, –11.4, 10.9, and 25.8 °C, respectively. The temperature hysteresis for the Cu-Al-Mn and Cu-Al-Mn-Ti alloys before and after quenching is shown in Table 4, and can be ranged

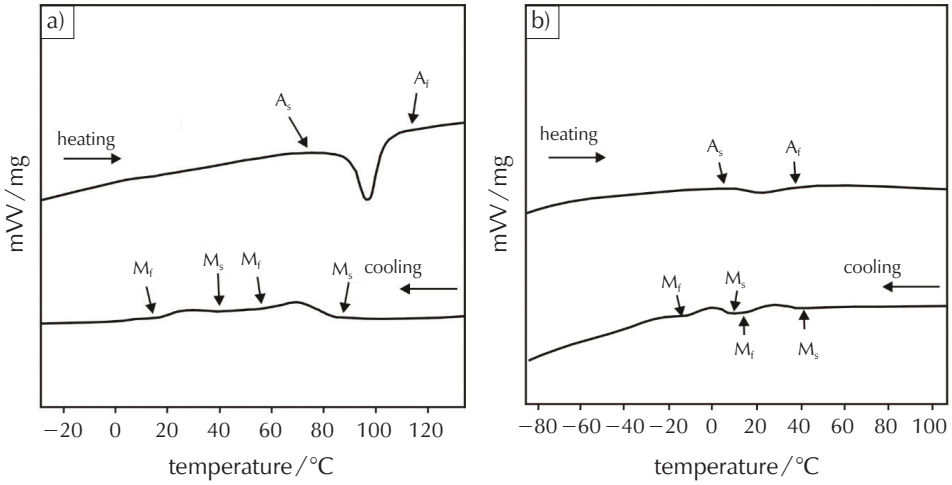

Fig. 8 – DSC thermograms of Cu-Al-Mn (a), and Cu-Al-Mn-Ti (b) shape memory ribbons before quenching

Slika 8 – DSC termogrami Cu-Al-Mn (a) i Cu-Al-Mn-Ti (b) traka s prisjetljivosti oblika prije kaljenja

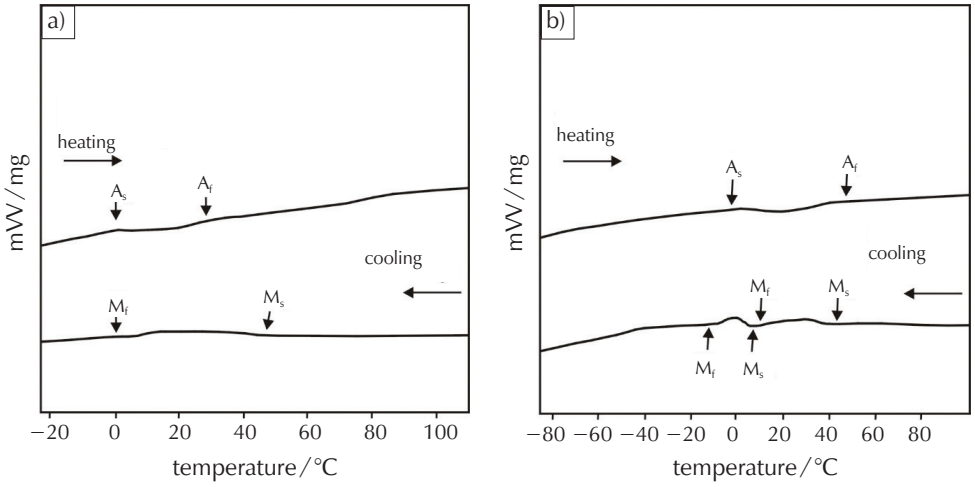

Fig. 9 – DSC thermograms of Cu-Al-Mn (a), and Cu-Al-Mn-Ti (b) shape memory ribbons after quenching

Slika 9 – DSC termogrami Cu-Al-Mn (a) i Cu-Al-Mn-Ti (b) traka s prisjetljivosti oblika nakon kaljenja

Table 4 – Phase transformation temperatures and temperature hysteresis of Cu-Al-Mn and Cu-Al-Mn-Ti alloys before and after quenching

Tablica 4 – Temperature faznih transformacija i temperaturna histereza Cu-Al-Mn i Cu-Al-Mn-Ti legura prije i nakon kaljenja

Alloy Legura	State Stanje	Transformation temperature / °C Temperatura transformacije / °C				Temperature hysteresis ΔT_H / °C Temperaturna histereza ΔT_H / °C
		A_s	A_f	M_s	M_f	
Cu-Al-Mn	casted lijevano	89.06	103.43	82.98	52.58	50.85
				45.77	12.39	91.04
Cu-Al-Mn-Ti	casted lijevano	11.31	39.13	37.23	16.25	22.88
				7.24	–12.10	51.23
Cu-Al-Mn	quenched kaljeno	8.04	33.35	39.60	5.46	27.89
Cu-Al-Mn-Ti	quenched kaljeno	8.33	34.08	37.57	8.25	25.83
				5.23	–9.57	43.65

from 22.88 to 91.04 °C. The change in temperature hysteresis is important to determine SME, and whenever the hysteresis is narrow, SME is high. According to *Canbay et al.,*[12] temperature hysteresis proceeds from the absorption of the internal energy described by three mechanisms: (i) dissipation of energy due to internal friction, (ii) storage of energy, and (iii) heat transfers due to the latent heat of phase change.

The research of electrical resistance was performed up to 200 °C. Electrical resistance versus temperature for Cu-Al-Mn alloy before quenching is shown in Fig. 10. The Cu-Al-Mn alloy before quenching shows changes in the electrical resistance curve with temperature change, *i.e.*, during the heating and cooling processes. These changes of electrical resistance are visible as deviations of linearity, and are observed as endothermic and exothermic peaks for Cu-Al-Mn before quenching, *i.e.*, only in Fig. 10a. These peaks can be caused by phase transformation. On the heating curve, one temperature interval of microstructural change is seen between 80 and 120 °C with peak maximum at 104.2 °C. This microstructural change can be caused by formation of austenite (A_s and A_f temperatures). On the other side, the cooling curve shows one exothermic peak, and this peak represents a martensitic transformation with M_s = 105 °C and M_f = 75 °C with peak maximum at 86.4 °C. The temperatures at which deviations of linearity appeared are only visible on the curve for the as-cast Cu-Al-Mn alloy (Fig. 10a). Other studied samples show behaviour similar to Fig. 10b, *i.e.*, phase transformations are not visible on the curves. This is expected and in accordance with DSC results. DSC results (Table 4) show temperatures of phase transformations for the Cu-Al-Mn-Ti alloy before and after quenching below 40 °C. The device used for electrical resistance measurement cannot detect martensite transformation at such low temperatures.

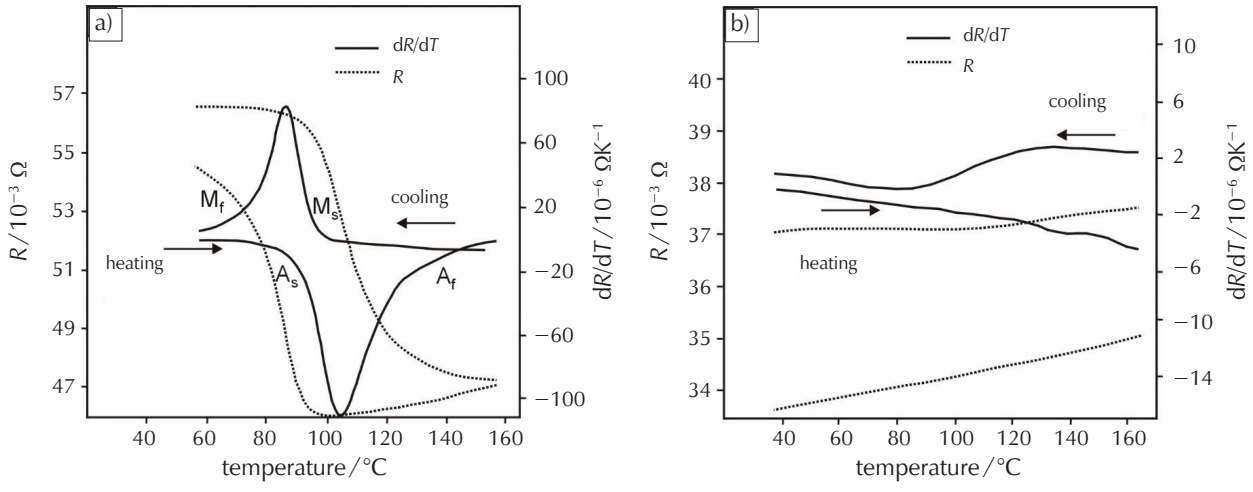

Fig. 10 – Electrical resistance *vs.* temperature of Cu-Al-Mn (a), and Cu-Al-Mn-Ti (b) shape memory ribbons before quenching

Slika 10 – Električni otpor u ovisnosti o temperaturi Cu-Al-Mn (a) i Cu-Al-Mn-Ti (b) traka s prisjetljivosti oblika prije kaljenja

4 Conclusions

The influence of quenching on microstructure and thermal properties of ductile Cu-Al-Mn and Cu-Al-Mn-Ti shape memory alloys were investigated. The obtained results suggest the following conclusions:

- Optical micrographs of the Cu-Al-Mn alloy before and after quenching showed the presence of a martensitic microstructure, while in Cu-Al-Mn-Ti alloy, the formation of martensite before quenching was not detected. Optical micrographs of Cu-Al-Mn-Ti alloy after quenching show that martensitic microstructure was achieved.
- SEM and XRD analysis of Cu-Al-Mn alloy before and after quenching showed the presence of the lath type (β_1') martensite with thin plates, and partial regions of the untransformed β phase. Before quenching, Cu-Al-Mn-Ti alloy consisted of a two-phase region of $\alpha + \beta_1$. After quenching, a formation of martensites (β_1' and γ_1') and austenite (β_1) was observed.
- DSC results indicate that the transformation temperatures for austenite and martensite microstructures vary with quenching and addition of titanium. After quenching of Cu-Al-Mn, transformation start and finish temperatures were at significantly lower values than before quenching, while for Cu-Al-Mn-Ti, they were similar. The Cu-Al-Mn-Ti alloy obtained lower values of transformation temperatures than Cu-Al-Mn.
- Martensite start and finish temperatures obtained by DSC analysis for the Cu-Al-Mn alloy after quenching were in range from 37.23 °C to –12.10 °C, and for Cu-Al-Mn-Ti after quenching, the values of transformation temperatures were similar.
- Only for the Cu-Al-Mn alloy before quenching did we see a change in peaks on the electrical resistance vs. temperature curve during heating and cooling. Martensitic transformation started at 105 °C and finished at 75 °C with peak maximum at 86.4 °C. For other studied samples, phase transformations were not visible on the electrical resistance vs. temperature curves because the device used for electrical resistance measurement cannot detect martensite transformation below and slightly above room temperature.

ACKNOWLEDGEMENTS

This work has been fully supported by Croatian Science Foundation under the project IP-2014-09-3405.

List of abbreviations and symbols
Popis kratica i simbola

A_s – austenite start temperature, °C
– temperatura početka austenitne transformacije, °C

A_f – austenite finish temperature, °C
– temperatura završetka austenitne transformacije, °C

A2 – form of crystal structure
– oblik kristalne strukture

B2 – form of crystal structure
– oblik kristalne strukture

DSC – differential scanning calorimetry
– diferencijalna pretražna kalorimetrija

EDS – energy dispersive spectroscopy
– energetski disperzivna spektroskopija

M_f – martensite finish temperature, °C
– temperatura završetka martenzitne transformacije, °C

M_s – martensite start temperature, °C
– temperatura početka martenzitne transformacije, °C

OM – optical microscopy
– optička mikroskopija

SEM – scanning electron microscopy
– pretražna elektronska mikroskopija

XRD – X-ray diffraction
– rendgenska difrakcija

2H – form of crystal structure
– oblik kristalne strukture

18R – form of crystal structure
– oblik kristalne strukture

α – phase, primary solid solution, FCC crystal structure
– faza, primarna čvrsta otopina, PCK strukture

β – austenite phase
– austenitna faza

β_1' – martensite phase
– martenzitna faza

γ – equilibrium phase
– ravnotežna faza

γ_1' – martensite phase
– martenzitna faza

References
Literatura

1. *Y. Sutou, T. Omori, J. J. Wang, R. Kainuma, K. Ishida*, Characteristics of Cu-Al-Mn based shape memory alloys and their application, Mater. Sci. Eng. **A378** (2004) 278–282, doi: https://doi.org/10.1016/j.msea.2003.12.048.
2. *N. Mali, A. Mali*, A review on shape memory alloy and its application in civil engineering, Int. J. Adv. Res. Sci. Eng. Technol. **4** (2017) 4395–4404.
3. *I. N. Quader, M. Kök, F. Dagdelen, Y. Aydogdu*, A review of smart materials: researches and applications, ECJSE **6** (2019) 755–788, doi: https://doi.org/10.31202/ecjse.562177.
4. *A. Hasnat, S. T. Ahmed, H. Ahmed*, A review of utilizing shape memory alloy in structural safety, AIUB J. Sci. Eng. **19** (2020) 116–125, doi: https://doi.org/10.53799/ajse.v19i3.111.
5. *H. Huang, Y.-Z. Zhu, W.-S. Chang*, Comparison of bending fatigue of NiTi and CuAlMn shape memory alloy bars, Adv. Mater. Sci. Eng. **2020** (2020) 8024803, doi: https://doi.org/10.1155/2020/8024803.
6. *P. Kumar, A. Kumar Jain, S. Hussain, A. Pandey, R. Dasgupta*, Changes in the properties of Cu-Al-Mn shape memory alloy due to quaternary addition of different elements, Rev. Mater. **20** (2015) 284–292, doi: https://doi.org/10.1590/S1517-707620150001.0028.
7. *U. Sari, T. Kirindi, F. Ozcan, M. Dikici*, Effect of aging on the microstructure of a Cu-Al-Ni-Mn shape memory alloy, Int. J. Min. Met. Mater. **18** (2011) 430–436, doi: https://doi.

org/10.1007/s12613-011-0458-1.

8. *R. Dasgupta, A. K. Jain, P. Kumar, S. Hussain, A. Pandey*, Role of alloying additions on the properties of Cu-Al-Mn shape memory alloys, J. Alloy. Compd. **620** (2015) 60–66, doi: https://doi.org/10.1016/j.jallcom.2014.09.047.
9. *L. S. Silva, R. A. G. Silva*, Alloys-by-design: Role of atomic properties on the phase equilibria of CuAlMn-based alloys, Mater. Charact. **163** (2020) 110304, doi: https://doi.org/10.1016/j.matchar.2020.110304.
10. *A. C. Kneissl, E. Unterweger, M. Bruncko, G. Lojen, K. Mehrabi, H. Scherngell*, Microstructure and properties of NiTi and CuAlNi shape memory alloys, MJoM **14** (2008) 89–100, doi: https://doi.org/10.3139/146.110147.
11. *S. Kožuh, M. Gojić, I. Ivanić, T. Holjevac Grgurić, B. Kosec, I. Anžel*, The effect of heat treatment on the microstructure and mechanical properties of Cu-Al-Mn shape memory alloy, Kem. Ind. **67** (2018) 11−17, doi: https://doi.org/10.15255/KUI.2017.025.
12. *C. A. Canbay, Z. Karagoz, F. Yakuphanoglu*, Controlling of transformation temperatures of Cu-Al-Mn shape memory alloys by chemical composition, Acta Phys. Pol. A **125** (2014) 1163–1166, doi: https://doi.org/10.12693/APhysPolA.125.1163.
13. *U. S. Mallik, V. Sampath*, Influence of aluminium and manganese concentration on the shape memory characteristics of Cu-Al-Mn shape memory alloys, J. Alloy. Compd. **459** (2008) 142–147, doi: https://doi.org/0.1016/j.jallcom.2007.04.254.
14. *C. A. Canbay, A. Dere,* Fabrication and characterization of ternary CuAlMn shape memory alloy with novel operation temperatures, J. Mater. Electron. Device. **6** (2021) 22–27.
15. *C. A. Canbay, S. Güdeloğlu*, Effects of aging temperature on microstructure and thermal properties of CuAlMn shape memory alloys, J. Nat. Appl. Sci. **21** (2017) 861–865, doi: https://doi.org/10.19113/sdufbed.49794.
16. *U. S. Mallik, V. Sampath*, Influence of quaternary alloying additions on transformation temperatures and shape memory properties of Cu-Al-Mn shape memory alloy, J. Alloy. Compd. **469** (2009) 156–163, doi: https://doi.org/10.1016/j.jallcom.2008.01.128.
17. *O. Adiguzel*, Smart materials and the influence of atom sizes on martensite microstructures in copper-based shape memory alloys, J. Mater. Process. Tech. **185** (2007) 120–124, doi: https://doi.org/10.1016/j.jmatprotec.2006.03.111.
18. *U. S. Mallik, V. Sampath*, Effect of alloying on microstructure and shape memory characteristics of Cu-Al-Mn shape memory alloys, Mat. Sci. Eng. A – Struct. **481-482** (2008) 680–683, doi: https://doi.org/10.1016/j.msea.2006.10.212.
19. *A. Mielczarek, N. Kopp, W. Riehemann*, Ageing effects after heat treatment in Cu-Al-Mn shape memory alloys, Mat. Sci. Eng. A – Struct. **521-522** (2009) 182–185, doi: https://doi.org/10.1016/j.msea.2008.10.066.
20. *S. Hussain, A. K. Jain, M. A. Ansari, A. Pandey, R. Dasgupta*, Study of effect of Fe, Cr and Ti on the martensite phase formation in Cu-12,5wt%Al-5wt%Mn SMA, Adv. Mater. Proceedings **2** (2017) 22–25, doi: https://doi.org/10.5185/amp.2017/106.
21. *Y. E. Gerdan, E. Aldirmaz, M. Guler, H. Tanak, E. Guler*, Martensitic transformation and magnetic properties of the CuAl, CuAlMn, and CuAlMnZn alloys, J. Supercond. Nov. Magn. **31** (2018) 3919–3923, doi: https://doi.org/10.1007/S10948-018-4658-Z.
22. *N. S. Saud, E. Hamzah, T. Abubakar, M. K. Ibrahim, A. Bahador*, Effect of a fourth alloying elements on the microstructure and mechanical properties of Cu-Al-Ni shape memory alloys, J. Mater. Res. **30** (2015) 2258–2269, doi: https://doi.org/10.1557/jmr.2015.196.
23. *P. Yong, X. Zhu, J. Yanlin, Z. Rui, Y. Jiang, Q. Wenting, L. Zhou*, Hot deformation behaviour of CuAlMn shape memory alloy, J. Alloy. Compd. **845** (2020) 156161, doi: https://doi.org/10.1016/j.jallcom.2020.156161.
24. *J. Miettinen*, Thermodynamic description of the Cu-Al-Mn system in the copper-rich corner, Calphad **27** (2003) 103–114, doi: https://doi.org/10.1016/S0364-5916(03)00035-X.
25. *Y. Sutou, T. Omori, R. Kainuma, K. Ishida*, Ductile Cu-Al-Mn based shape memory alloys: general properties and applications, Mater. Sci. Tech. **24** (2008) 896–901, doi: https://doi.org/10.1179/174328408X302567.
26. *L. Zhou, J. Lan, J. Liu, X. Li, B. Shi, S. Zheng*, Effect of gradient heat treatment on microstructure and properties of Cu-Al-Mn shape memory alloy, Materials **12** (2019) 2505, doi: https://doi.org/10.3390/ma12162505.
27. *N. Zárubová, V. Novák*, Phase stability of CuAlMn shape memory alloy, Mater. Sci. Tech. A **378** (2004) 216–221, https://doi.org/doi: 10.1016/j.msea.2003.10.346.
28. *J. Liu, Z. H. Chen, H. Huang, J. Xie*, Microstructure and superelasticity control by rolling and heat treatment in columnar-grained Cu-Al-Mn shape memory alloy, Mat. Sci. Eng. A – Struct. **696** (2017) 315–322, doi: https://doi.org/10.1016/j.msea.2017.04.085.

SAŽETAK

Utjecaj toplinske obrade na mikrostrukturu i toplinska svojstva traka s prisjetljivosti oblika na bazi bakra

Stjepan Kožuh,[a*] *Ivana Ivanić*,[a] *Tamara Holjevac Grgurić*[b] i *Mirko Gojić*[a]

Cilj rada bio je istražiti promjene u mikrostrukturi, temperaturama transformacije i toplinskim svojstvima nastale uslijed kaljenja Cu-Al-Mn i Cu-Al-Mn-Ti legura u obliku trake. U radu su prikazani rezultati mikrostrukturne analize i toplinskih svojstava Cu-Al-Mn i Cu-Al-Mn-Ti legura s prisjetljivosti oblika proizvedenih u obliku trake postupkom *melt spinning*. Mikrostrukturna analiza je provedena prije i nakon kaljenja. Nakon lijevanja istraživane legure su žarene pri 900 °C u trajanju 30 minuta, nakon čega je slijedilo kaljenje u vodi. Mikrostrukturna analiza je provedena optičkim i pretražnim elektronskim mikroskopom opremljenim energetsko disperzijskim spektroskopom te rendgenom. Termodinamički proračun ternarnog Cu-Al-Mn sustava proveden je u ravnotežnim uvjetima pomoću Thermo-Calc 5 programskog paketa. Temperature fazne transformacije određene su diferencijalnom pretražnom kalorimetrijom i mjerenjem električnog otpora. Rezultati mikrostrukturne analize pokazuju prisutnost martenzitne mikrostrukture prije i nakon kaljenja Cu-Al-Mn legure, dok u Cu-Al-Mn-Ti leguri martenzitna mikrostruktura postoji samo nakon kaljenja. Temperature faznih transformacija smanjuju se nakon kaljenja i dodatka titana.

Ključne riječi
Cu-Al-Mn, Cu-Al-Mn-Ti, legure s prisjetljivosti oblika, mikrostrukturna karakterizacija, toplinska analiza, rendgenska spektroskopija

[a] *Sveučilište u Zagrebu, Metalurški fakultet, Aleja narodnih heroja 3, 44000 Sisak, Hrvatska*
[b] *Hrvatsko katoličko sveučilište, Ilica 242, 10000 Zagreb, Hrvatska*

Izvorni znanstveni rad
Prispjelo 16. veljače 2022.
Prihvaćeno 27. travnja 2022.